2014 IEEE International Conference on Robotics & Automation (ICRA)
Hong Kong Convention and Exhibition Center
May 31 - June 7, 2014. Hong Kong, China

Unified Hysteresis and Creep Compensation in AFM Tip Positioning with an Extended PI Model

Zhiyu Wang, Lianqing Liu, *Member*, *IEEE*, Zhidong Wang, Wenxue Wang, *Member*, *IEEE*

Abstract—**The nonlinearities such as hysteresis and creep are the major factors inherent in PZT actuation that affect the tip positioning precision and manipulation performance of the AFM system. In this study, an extended PI model is generalized by introducing a creep model to the basic hysteretic operator of the PI model at the inflexion point of the hysteresis loop. Unified compensation for hysteresis and creep can be implemented with the extended PI model. Experiment results demonstrate the validity and effectiveness of the extended PI model and it is implied that the inflexion creep compensation not only improves the tip positioning precision at the inflexion points on the hysteresis loops, but also the localization effectiveness during the whole process of PZT actuation.**

Keywords—***Hysteresis, Creep, Prandtl-Ishlinskii model, AFM, Pizeoelectric.***

I. Introduction

Atomic force microscopy (AFM) based robotic system becomes a powerful and promising tool in both nanofabrication and nanomanipulation areas due to its wide range of capabilities and applicability although AFM was originally invented for imaging and measuring matter at the nanoscale [1]. In nanofabrication, an AFM-based technique utilizing dynamic ploughing of a thin resist layer followed by pattern transfer of the lines into semiconductor through wet chemical etching was developed for fabricating ballistic quantum point contacts (QPCs) and resulted in promising subband separations [2]-[4], and the effect of geometric variations on the transport properties of QPCs was further investigated [5]. AFM-based probe anodic oxidation is another effective technique for fabricating nano structures on substrate [6] or nano devices by controlling the position of oxide dots precisely to combine nano parts [7], and this approach was latterly successfully applied to oxidative cutting and welding of carbon nanotube (CNT) by controlling the distribution of electric field on substrate surface and fabrication parameters such as bias voltage, tip-substrate distance and tip writing speed [8]. Furthermore, integrated with augmented reality interface, including real-time force and visual feedbacks, AFM-based robotic systems were developed for interactive nanomanipulation and nanoassembly with improved efficiency and effective [9], [10].

The nanomanipulation performance of the AFM-based robotic systems is significantly affected by the spatial uncertainties, which are caused by random drift and faulty visual display. Efforts have been put into reducing the effect of such uncertainties. On-line sensing and display with local scanning strategy was developed for drift compensation and faulty display correction [11], Kalman filter techniques were applied to drift estimation [12] and to a probabilistic localization algorithm for improving tip positioning precision in nanomanipulation [13], and a virtual nanohand strategy with stochastic prediction was developed for automatic and stable nanoparticle pushing without monitoring the dynamic interactions between the tip and nanoparticles during the whole pushing process [14]-[16].

Another type of major factors that affect the nanomanipulation performance with AFM are the complex system nonlinearities inherent in the piezoelectric ceramics tube (PZT) actuation. One of the main nonlinearities of PZT actuation is the hysteresis, which cause a multi-valued mapping between excitation voltage signal and displacement of PZT [17]-[19]. Many models have been proposed for the description and compensation of the nonlinear characteristics. One of the classical models is Preisach model to describe hysteresis with a basic relay hysteron in a stacked form, which shows excellent modeling accuracy with excitation voltage signal at low frequencies when the actuator is not subject to any load [17]. However Preisach model ignores the significant rate-dependent characteristic of PZT actuator that the displacement depends on the excitation voltages, and the modeling accuracy increasingly deteriorates as the load fluctuation applied to PZT actuator is relatively large and the range of frequencies of the voltage excitation get wider. Prandtl-Ishlinskii (PI) model stems from Preisach model, whose basic operator is a piecewise continuous closed loop with consideration of rate dependency [18], [19]. Compared with Preisach model, PI model has a simpler form and a smaller number of parameters, which makes it easier to compute the inverse of PI model for hysteresis compensation. Hence PI model is widely used for real time feedforward control in PZT actuation for hysteresis compensation.

Creep is another nonlinear characteristic in PZT actuation. When a driving voltage signal of PZT stands still, the

This worl is supported by the National Natural Science Foundation of China (Grant No. 61327014, 61304251), and the CAS/SAFEA International Partnership Program for Creative Research Teams.

Zhiyu Wang, Lianqing Liu, Zhidong Wang and Wenxue Wang are with the State Key Laboratory of Robotics, Shenyang Institute of Automation, Chinese Academy of Sciences (CAS), 110016, China.

Zhiyu Wang is also with the College of Electrical and Control Engineering, Liaoning Technical University, and University of Chinese Academy of Sciences, China

Zhidong Wang is also with the Dept. of Advanced Robotics, Chiba Institute of Technology, Japan.

Corresponding authors: **lqliu@sia.cn** (for AFM-based nanomanipulation) and **wangwenxue@sia.cn** (for hysteresis and creep compensation)

displacement of PZT keeps changing slowly and cannot be hold at a certain value. The creep effect deteriorates the PZT positioning in detection and manipulation. Several modified PI model were proposed for compensation of both creep and hysteresis [20], [21], in which the creep effects are described as a first order linear system. With these methods for hysteresis and creep compensation, the creep effects are considered for all the time during the whole PZT activation process and depend on the history of excitation voltage signal, which makes the computation of the inverse model difficult. In fact, the creep effect in PZT actuation is not uniform, and the creep compensation at every voltage excitation consumes a lot of time for computing the inverse model and hence encumbers the application of such compensation to AFM-based robotic system with high speed actuation. An extended PI model was proposed by introducing a creep parameter into the hysteresis operator to compensate for inflexion creep effects only at the turning point of the single hysteretic loop, which significantly increased the tip positioning precision [22].

In addition, closed-loop control strategies, such as sliding-surface control [23], Dahl Model-based control [24], iterative control [25], [26], can be applied to compensate for hysteresis and creep nonlinearities. However, compared with the PI model based feedforward control systems for hysteresis and creep compensation, the closed-loop control systems need extra sensors for measuring the PZT displacements and hence cause new noises and vibration in dynamic driving curve.

In this paper, the extended PI model proposed in [22] is generalized with consideration of multi-loop hysteresis, for which the inflexion creeps are modeled as a generalized function of time with magnitude depending on the value of the corresponding turning point of the driving voltage signal. Therefore the complete extended PI model can be used to the inflexion creeps at any turning point on the hysteretic loop. Furthermore, the number of parameters in the creep model has been greatly reduced into three, which mathematically reveal the relationship between the creep effect and its driving voltage in PZT actuation.

The paper is organized as follows. Section II briefly describes the inflexion creep through a PZT calibration experiment. Section III presents the generalized extended PI model by introduction of the inflexion creep model described as a function of time with magnitude depending on the turning voltage value as well as the inverse model. Section IV implements experiments for creep calibration and parameter identification of the extended PI model and its inverse, and then validate the effectiveness of hysteresis and creep compensation with the extended PI model. Section V concludes this paper with discussion.

II. Inflexion Creep and Hysteresis in PZT Actuation

The precise tip positioning is crucial for the effectiveness and performance of AFM-based nanomanipulation and nanofabrication. For those AFM systems with displacement sensors, the tip placement can be recorded in real time, and the tip position on the sample surface can be derived accordingly. In this case, the hysteresis and creep effects can be compensated with closed control strategies. However, the closed-loop control strategies do not work for those AFM systems that lack of displacement sensors. In this case, the tip position on the sample plane can be directly marked by the probe itself and a feedforward control strategy is required for hysteresis and creep compensation to improve tip positioning precision.

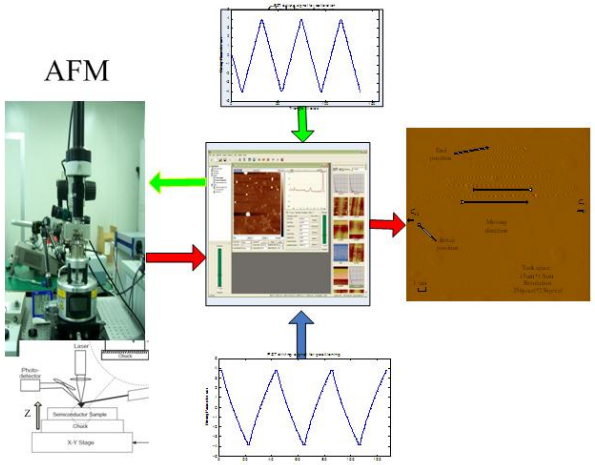

Fig.1. Using an Atomic Force Microscopy (AFM) system for PZT calibration.

The AFM system, Multimode, for nanomanipulaiton in this study is the one without displacement sensors, as shown in the left subplot of Figure 1. The probe movements along the three directions are independently driven by three pairs of electrodes in the PZT actuator. To study the simultaneous compensations for hysteresis and creep, a sample with flat surface is fixed on the platform upon the top of PZT actuator and under the probe for implementing calibration experiment. In this study, a piece of clean compact disc (CD) is chosen for the experiments for inflexion creep calibration and validation of hysteresis and creep compensation because CD surface is flat and soft enough for indenting with the AFM probe. The position of the probe on the sample surface, X-Y plane, and the height of the tip relative to the sample surface along the Z axis can be changed by driving the PZT through three driving voltages. The Multimode system can measure tiny distance difference on the sample surface with relatively high resolution in imaging process. The nonlinearities of hysteresis and creep of the PZT in the Multimode can be characterized through horizontal calibration with indentation by varying the excitation voltage for X-direction voltage, which is set as a triangle wave, as shown in the upper subplot of Figure 1. The triangle wave is fed into the AFM system through the control panel (the central subplot of Figure 1), and drives the PZT to move along a designed trajectory, indenting the substrate for recording the tip positions. The indenting result is then imaged by the scanning mode of the AFM system as shown in the right subplot of Figure 1. Based on the calibration data, the feedforward controller can be constructed with the nonlinearity compensations to realize the desired probe positioning and movement, as shown in the

bottom subplot of Figure 1. The experiments are implemented at a constant ambient temperature of 16 degree, which can restrain the thermal drift effect. The indentation marking the moving trajectory of the tip is imaged by the scanning mode of the AFM system as shown in Figure 2. The real position of the tip on the sample plane is recorded by the indentation. The horizontal displacement of AFM tip can be read out in pixels and translated into micrometer which is depicted as hysteresis loop as shown in Figure 3. The arrows in both Figure 2 and Figure 3 denote the moving directions of the tip on the sample plane.

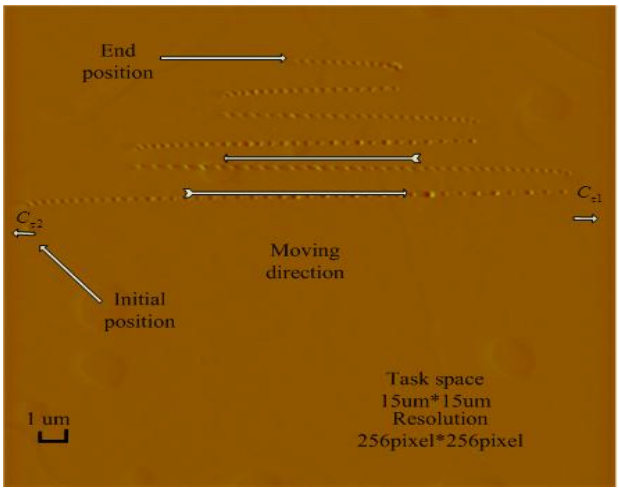

Fig.2. Indentation experimental results for characterizing the hysteresis and inflexion creep in PZT actuation.

Inflexion points are those excitation voltage values at which the driving signal changes the variation direction. At each inflexion point of the X-driving signal, the inflexion value stands still for a sampling period of milliseconds, and meanwhile the tip is moved for a certain distance along the Y direction to prevent the returning trajectory from overwriting the previously indented line. The creep taking place at the inflexion point is called inflexion creep, shown as in Figure 3.

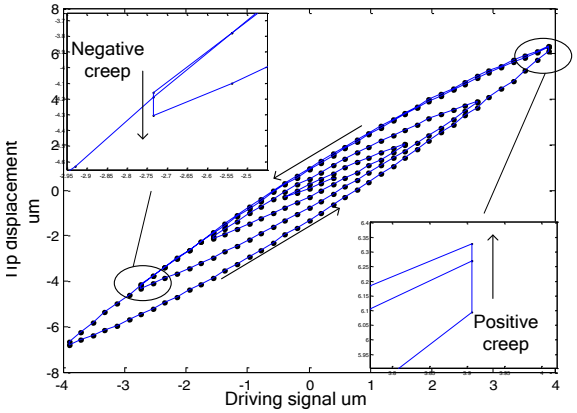

Fig.3. The displacement characteristics of AFM tip showing the hysteresis and creep effects.

Although the creeping time is about tens of milliseconds, the creep displacement in X-axis in this example is several tens nanometers, which is enough to cause the tip to lose nano-objects and hence deteriorates the performance and effectiveness of nanomanipulation. In this study, we focus on the simultaneous compensation of hysteresis and inflexion creep.

III. Mathematical Expression for the Inflexion Creep and the Extended PI Model

The inflexion creep can be modeled as the response of a first order linear system with a step function as input, which corresponds to the inflexion voltage [20], [21]. The magnitude of the creep depends on the inflexion voltage value. In this study, the calibration data shows that the creep magnitude is an exponential function of the inflexion voltage value. Therefore, the inflexion creep is mathematically described as follows:

$$C(u,t) = (1 - e^{\lambda(u)*t}) * M(u) \quad (1)$$

$$M(u) = a \times b^{u} \quad (2)$$

Where, both $\lambda(u)$ and $M(u)$ are the functions of inflexion voltage value u . PI model is time independent, while inflexion creep is a function of time, therefore the inflexion creep cannot be considered in PI. To implement simultaneous compensation of hysteresis and inflexion creep, an operator is introduced through the extension of the basic hysteretic operator of PI model by adding/subtracting the inflexion creep model. The new extended basic operator for both hysteresis and inflexion creep (called as *HC* operator) is expressed as follows:

$$HC_{ri}[u, x_{0i}](t) =$$

$$\begin{cases} \max\{u(t) - r_i, \min\{u(t) + r_i, x(t-T)\}\} + C_{ri}(u,T) \\ \qquad \text{if } u(t) = u(t-T) > u(t-2T) > 0; \\ \max\{u(t) - r_i, \min\{u(t) + r_i, x(t-T)\}\} - C_{ri}(u,T) \\ \qquad \text{if } u(t) = u(t-T) < u(t-2T) < 0; \\ \max\{u(t) - r_i, \min\{u(t) + r_i, x(t-T)\}\} \\ \qquad \text{if } u(t) \neq u(t-T); \end{cases} \quad (3)$$

$$r_i = \frac{i}{n+1}\|x\|_{\infty}, C_{ri}(u,T) = \frac{i}{n+1}C(u,T) \quad , \quad x_{0i} = 0$$

where $u(t)$ is a driving voltage and $HC_{ri}(t)$ is the output of the operators, $C(u,T) \geq 0$ is the inflexion creep function, $\vec{r} = (r_0, r_1, \cdots, r_n)$ is a threshold vector, and $\| \bullet \|$ denotes the usual Euclidean norm. The deduction is similar with the traditional PI model [18], [19]. $\vec{x}_0 = (x_{00}, x_{01}, \cdots, x_{0n})$ is a vector of initial values of the output.

With the basic operators in Eq. 3, the displacement output of the PZT actuation is expressed as follows:

$$Y(t) = HC[u, x_0](t) = \omega^T (HC_{r_0}[u, x_{00}](t); \cdots HC_{r_n}[u, x_{0n}](t)) \quad (4)$$

where $Y(t)$ is the displacement output, $HC_{r_i}[u, x_{0i}](t)$ is the ith *HC* operator, $\vec{\omega} = (\omega_0, \omega_1, \cdots, \omega_n)^T$ is a weight vector. The output is a weighted sum of a series of *HC* operators with corresponding threshold parameter r . Since *HC* operator stems from the traditional hysteretic operator of PI model, the parameters of the forward model and its inverse can be obtained in the same method. Therefore, the parameter $\vec{\omega}$ of the extended

PI model can be calculated by Least Square Method described as follows:

$$\vec{\omega} = (HC * HC^T)^{-1} HC * X \tag{5}$$

where, X is a vector of calibration data i.e. the PZT displacements.

In [18] and [19], it has been proven that the hysteresis operator of PI is piecewise continuous and invertible, and the inverse of PI model is also modeled as the weight sum of PI operators, which is written as follows:

$$H^{-1}[u', x'_0](t) = \omega'^T H_{r'}[u', x'_0](t) \tag{6}$$

$$H_{r'}[u, x_0](t)^T = (H_{r_0'}[u, x_{00}](t) \cdot\cdot H_{r_n'}[u, x_{0n}](t)) \tag{7}$$

where the superscript "'" indicates that the corresponding parameter belongs to the inverse of PI model. The input signal u' is the expected displacement and the output x' is the driving signal for the PZT actuation. Likely, The inverse of the extended PI model has the similar form with its forward model, and can be expressed by Eq. 6 and Eq. 7, and the parameters of the inverse model can be calculated through the following equations [18], [19]:

$$r_i' = \sum_{j=0}^{i} \omega_j (r_i - r_j); \tag{8}$$

$$\omega_0' = \frac{1}{\omega_0} \tag{9}$$

$$\omega_i' = \frac{\omega_i}{(\omega_0 + \sum_{j=1}^{i} \omega_j)(\omega_0 + \sum_{j=1}^{i-1} \omega_j)} \tag{10}$$

$$x'_{0i} = \sum_{j=0}^{i} \omega_j x_{0i} + \sum_{j=i+1}^{n} \omega_j x_{0i} \tag{11}$$

IV. Experiments for Calibration and Validation of Hysteresis and Inflexion Creep Compensation

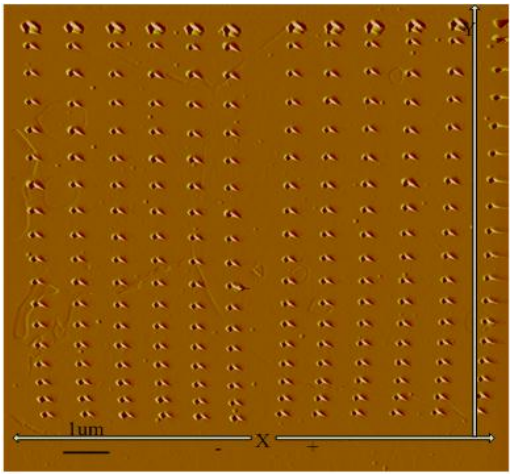

Fig.4. Inflexion creep calibration using the AFM system.

The inflexion creep takes place at the inflexion points of driving signal, with magnitude depending on the inflexion voltage value. Then the inflexion creep can be calibrated at different inflexion voltage for a certain time by the tip indentation method. As shown in Figure 4, each column of indentations indicate an inflexion creep trajectory at a certain inflexion voltage value in the X-direction, with moving the tip in Y-direction within the creeping time. For example, in the rightmost column of indentation, the voltage in the X-direction holds still and the tip moves in the Y-direction for indenting the substrate within creeping time. It can be seen that the X-coordinates of the indented points gradually varies in the same direction, indicating the creep effect of the PZT actuator in the X-direction. It is obvious that the creep effects take place at any excitation voltage value.

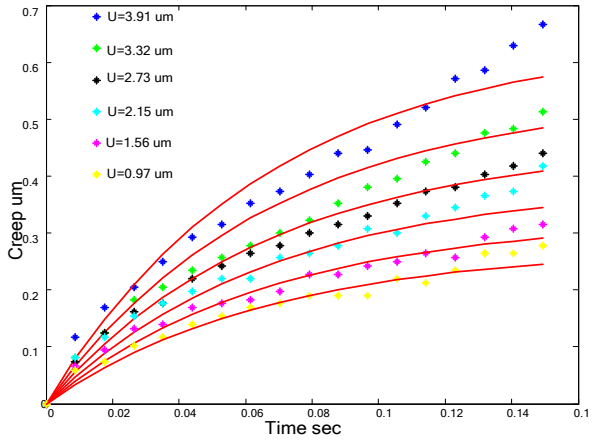

Fig. 5. Calibrated inflexion creep curves at different inflexion points.

The creep direction is consistent with the variation direction of the driving signal. Therefore the inflexion creep can be divided into positive creep and negative creep, taking place at the right and left inflexion points on the hysteresis loops respectively, corresponding to the creep trajectories on the right part and the left part in Figure 4. For the simplicity of study, we assume that the positive and negative creeps are symmetric. So the inflexion creep trajectories with different inflexion voltages in Figure 4 are extracted and displayed in Figure 5, with the dotted curves representing the X-coordinates and the solid curves fitting the corresponding trajectories.

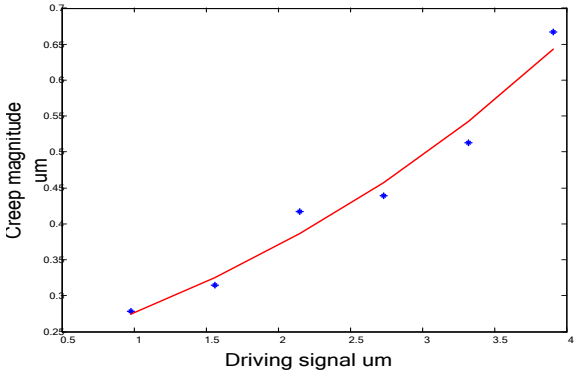

Fig. 6. Calibrated creep magnitudes at different inflexion points.

Based on the inflexion creep trajectories, the parameters of the creep model can be easily identified. In this study, the parameter $\lambda(u)$ is set to a constant value based on the experimental data. The magnitude of creep effect $M(u)$ at a

certain inflexion voltage represents how far the creep goes as time elapses. Hence the magnitudes of the inflexion creeps are set to the values that the fitting curves of creep trajectories converge. Then the magnitude curve of inflexion creep can be achieved by fitting these magnitude values, as shown in Figure 6 where the dots represent the creep magnitude values of the creep trajectories and the solid curve is the creep magnitude as a function of inflexion voltage values.

With estimated parameters of the creep model, the fitting curve for the displacement data in Figure 3 can be computed according to Eq. 3~Eq. 5, as shown in Figure 7 and the estimated parameters for the forward model are listed in the left column of Table 1. The blue curve is the original experimental data from Figure 3, and the red line is its fitting curve by the extended PI model depicted in Eq. 3 and Eq. 4. The subplots in the figure are the enlargements of the area containing a local inflexion creep. On the multi-loop hysteresis displacement curve, the fitting curve with the inflexion creep model follows the creep displacement at every inflexion points of driving signal. The fitting errors are shown in Figure 8.

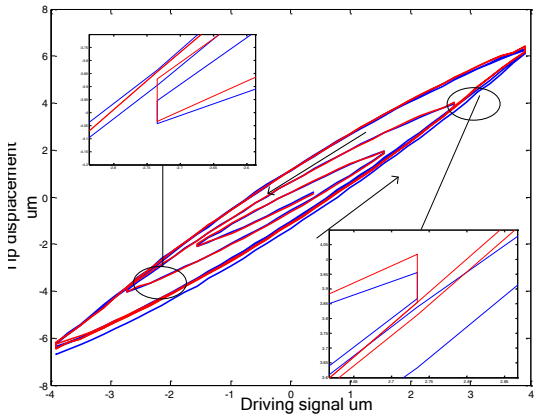

Fig 7. Curve fitting with hysteresis and creep compensations using the extended PI model for the hysteresis loops.

TABLE I. WEIGHT VECTOR ω OF THE EXTENDED PI MODEL

ω	Forward model	inverse model
ω_0	0.793172317251542	1.26076008737313
ω_1	0.442071134534941	-0.451203073689922
ω_2	0.020794338851802	-0.0134026244973307
ω_3	0.106723904368183	-0.0623503765956520
ω_4	0.065040417898840	-0.0334268448010620
ω_5	0.135513334974812	-0.0607110010177552
ω_6	0.063105484487529	-0.0248191858337850
ω_7	0.094334675503508	-0.0337069309353110
ω_8	-0.04126196165719	0.0142775047197761
ω_9	0.198065016399163	-0.0628110269408285
ω_{10}	0.083849403629362	-0.0227687142171887
ω_{11}	0.259960105191838	-0.0596648017871405
ω_{12}	-0.36562028779604	0.0886932904922409

Similarly, the weight vector of the inverse model can be computed using Eq. 8~Eq. 11, as listed the right column of the Table.1 With these parameters, the hysteresis and creep can be compensated with the inverse of the extended PI model depicted in Eq. 6 and Eq. 7.

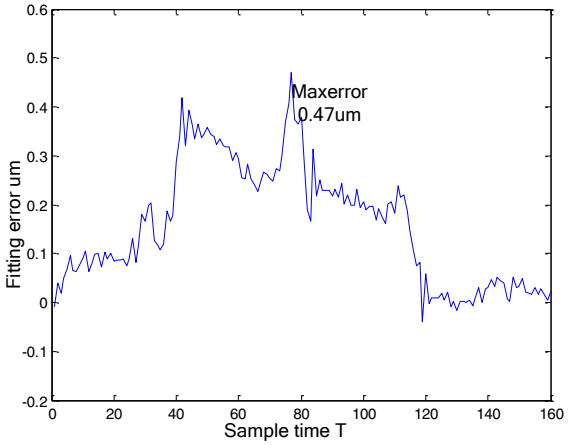

Fig 8. The distribution of errors between the fitting curve and the multi-loop hysteresis.

The feedforward control system is constructed with nonlinearity compensator by the inverse of the PI model or extended PI model. With estimated parameters of the inverse model, the desired voltage signal for expected tip positions is generated and then fed into the AFM system. In this study, two groups of localization experiments are carried out to compare the compensation performance of the extended PI model and the original PI model. The tip positions are expected to distribute uniformly in the X-direction.

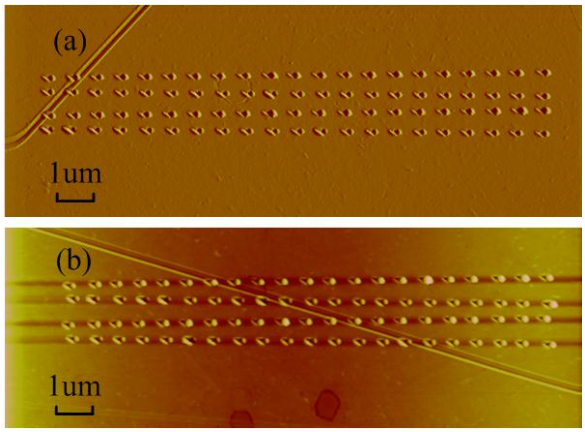

Fig.9. The indentation array comparison.

The indentation arrays on the CD sample surfaces are shown in Figure 9, where the top subfigure is for the indenting experiment with the hysteresis and inflexion creep compensation using the extended PI model, and the bottom subfigure for the indenting experiment with only the hysteresis compensation using the traditional PI model.

The statistical distribution of error between the expected tip position and the actual indenting position is shown in Figure 10, where the blue curve is the positioning error distribution with both hysteresis and creep compensations using the extended PI model, and the red curve is the positioning error with only the hysteresis compensation. It is

obvious that the inflexion creep compensation not only improves the tip positioning precision at the inflexion points on the hysteresis loops, but also the localization effectiveness during the whole process of PZT actuation.

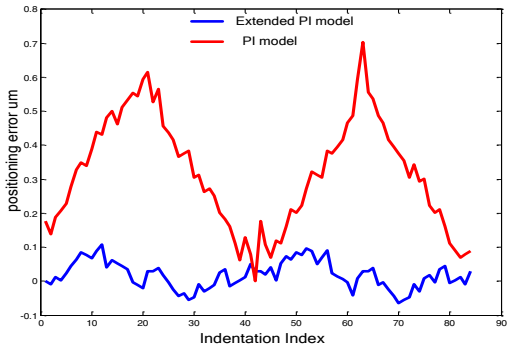

Fig.10. positioning error distribution comparison.

V. Discussion and Conclusion

Hysteresis and creep are the two main nonlinearities inherent in PZT actuation and significantly affected AFM-based nanomanipulation. In this study, an extended PI model has been developed by adding (subtracting) a creep model to (from) the basic hysteretic operators of the PI model. The model is the generalization of the work proposed in [22]. By comparison of the compensation performances of the extended PI model and PI model, it shows that the extended PI model can better compensate for the effects of hysteresis and creep nonlinearities than the PI model, and the inflexion creep compensation not only improves the tip positioning precision at the inflexion points on the hysteresis loops, but also the localization effectiveness during the whole process of PZT actuation.

The proposed extended PI model in this study has a relatively simpler structure and less parameters than the compensation methods in [20], [21] , in which the creep model depends on the history of input signal and the creep effects are compensated through the whole process of PZT actuation. Therefore the hysteresis and creep compensation with the extended PI model will consume less time, which is especially meaningful for the AFM-based nanomanipulation requiring high speed actuation.

Incorporated with the local scanning strategy [11] or the virtual nanohand strategy [14]-[16], the extended PI model can improve the scanning accuracy, and therefore reduce the effect of the spatial uncertainties caused by the thermal drift.

References

[1] G. Binnig and C. F. Quate, "Atomic force Microscope," *Appl Phys Lett*, 56(9): 930-933, 1986.

[2] B. Klehn and U. Kunze, "SiO2 and Si nanoscale patterning with an atomic force microscope," *J. Appl. Phys.*, 85(7): 3897-3903,1999.

[3] B. Klehn, S. Skaberna and U. Kunze, "Plowing on the Sub-50nm Scale:Nanolithography Using Scanning Force Microscopy," *Superlattices Microstruct*, 11(17): 1473-1475, 1999.

[4] S. Skaberna, M. Versen, B. Klehn, et al., "Fabrication of a quantum point contact by the dynamic plowing technicque and wet-chemical etching" *Ultramicroscopy*, 82: 153-210, 2000.

[5] G. Apetrii, S.F. Fischer, U. Kunze, et al. "Influence of processing parameters on the transport properties of quantum pointcontacts fabricated with an atomic force microscope," *Semicond Sci Technol*, 17:735-744, 2002.

[6] H. C. Day, and D. R. Allee, "Selective area oxidation of silicon with a scanning force microscope," *Appl Phys Lett*, 62(21): 2691-2693, 1993.

[7] E. S. Snow, W. H. Juan, S. W. Pang, et al. "Si nanostructures fabricated by anodic oxidation with an atomic force microscope and etching with an electron cyclotron resonance source," *Appl Phys Lett,* 66(14): 1729-1731, 1995.

[8] N. Jiao, Y Wang, N. Xi, et al., "AFM based anodic oxidation and its application to oxidative cutting and welding of CNT, " *Journal of Sci China Ser E-Tech Sci*, 52(11): 3149-3157, 2009.

[9] H. Chen, N. Xi and G. Li, "CAD-Guided Automated Nanoassembly Using Atomic Force Microscopy-Based Nonrobotics," *IEEE transactions on automation science and engineering,* 3(3):208-217, 2006.

[10] G. Li, N. Xi, H. Chen, et al. ,"Videolized Atomic Force Microscopy for Interactive Nanomanipulation and Nanoassembly," *IEEE transactions on nanotechnology*, 4(5):605-615, 2005.

[11] L. Liu, N. Xi, Y. Wang, et al., "Drift Compensation and Faulty Display Correction in Robotic Nano Manipulation" *Journal of Nanoscience and Nanotechnology*, 10: 7010-7014, 2010.

[12] B. Mokaberi and A. A Requicha, "Drift compensation for automatic nanomanipulation with scanning probe microscopes," *IEEE Trans. Autom. Sci. Eng.*, 3(3), 199-207, 2006.

[13] S. Yuan, L.Liu, Z. Wang, et al., "A Probabilistic Approach for On-line Positioning in Nano Manipulations" *World Congress on Intelligent Control and Automation,* 450-455,2010.

[14] Z.. Wang, L.. Liu, Z. Wang et al., "Virtual nano-hand: A stable pushing strategy in AFM based sensorless nanomanipulation," *Proc. IEEE Int.Robio Conf.,* 1409-1414, 2011.

[15] J. Hou, L. Liu, Z. Wang et al., "AFM-Based Robotic Nano-Hand for Stable Manipulation at Nanoscale," *IEEE Trans. Autom. Sci. Eng.,* 10:285-295, 2013.

[16] Z.Wang, L.Liu, Y..Wang, et al., "Stable nanomanipulation using Atomic Force Microscopy," *Nanotechnology*, 7(4):6-11, 2013.

[17] H. Hu and R. B Mrad, "On the classical Preisach model for hysteresis in piezoceramic actuators," *Mechatronics*, 13:85-94, 2003.

[18] Kuhnen K and Janocha H, "Inverse feedforward controller for complex hysteretic nonlinearities in smart-material systems," *Control and Intelligent Systems*, 2001

[19] K. Kuhnen and H. Janocha, "Complex hysteresis modeling of a broad class of hysteretic nonlinearities," *Proc. 8th Int. Conf. New Actuators,* Bremen, Germany, 688-691, 2002.

[20] P. Krejci and K. Kuhnen, "Inverse control of systems with hysteresis and creep," *Control Theory and Applications*, 148(3):4008-4009, 2001.

[21] B. Mokaberi and A. A Requicha, "Compensation of Scanner Creep and Hysteresis for AFM Nanomanipulation," *IEEE Trans. Autom. Sci. Eng.*, 5(2):197-206, 2008.

[22] Z. Wang, L. Liu, Z. Wang et al., "An extended PI model for hysteresis and creep compensation in AFM based nanomanipulation," *Proc. IEEE Int.Robio Conf.*, 992-997, 2010.

[23] H. J. Shieh and P.K. Huang, "Precise tracking of a piezoelectric positioning stage via a filtering-type sliding-surface control with chattering alleviation," *IET Control Theory and Applications*, 1(3), 586-594, 2007.

[24] Q. Xu and Y. Li, "Dahl Model-Based Hysteresis Compensation and Precise Positioning Control of an XY ParallelMicromanipulator with Piezoelectric Actuation," *ASME Transactions on Dynamics, System, Measurement, and Control*, 132(2): 041011, 2010.

[25] Y. Wu and Q. Zou "Iterative control approach to compensate for both the hysteresis and the dynamics effects of piezo actuators," *IEEE Trans Control Syst Technol*, 15(5):906-915, 2007.

[26] B. E. Helfrich, C. Lee, D. A. Bristow, et al. "Combined H_∞ -feedback control and iterative learning control design with application to nanopositioning systems," *IEEE Trans Control Syst Technol.*, 18(2):336-351, 2010.